Accepted Manuscript
Version of record at: https://doi.org/10.1093/insilicoplants/diac008

Evaluation of Brace Root Parameters and Its Effect on the Stiffness of Maize

Shaymaa K. Obayes[1*], Luke Timber[1], Monique Head[2], Erin E. Sparks[3]

Graduate Research Assistant, Department of Civil & Environmental Engineering, University of Delaware

Associate Professor, Department of Civil & Environmental Engineering, University of Delaware

Assistant Professor, Department of Plant and Soil Sciences, University of Delaware

**Corresponding Author: +1 (302) 384-2445 shko@udel.edu*

127 The Green, 360H DuPont Hall, Newark, DE 19716

Authors Contribution:

Shaymaa Obayes: field test setup, data analysis, manuscript writing

Luke Timber: field test setup and calibration, post-processing data

Monique Head: field test setup, data analysis, manuscript writing and editing

Erin E. Sparks: project management, field test setup, data analysis, manuscript writing and editing

---

Monique Head[2] and Erin E. Sparks[3] should be considered joint senior authors.

Abstract

Plant mechanical failure (lodging) causes significant yield loss for crops such as maize. Understanding this failure has relied on static measurements of plant biomechanics. In this study, digital image correlation techniques are used to capture dynamic motion to understand the plant mechanical behavior of maize stalks in the presence and absence of brace roots, which are stem-borne aerial roots known to stabilize the maize stalks. The data show that brace roots function to secure the maize stalk, limiting both deflection and uplift. A finite element (FE) model is developed using ABAQUS software to validate the non-contact, video-based measured deflections captured by the dynamic motion and confirm the linear elastic behavior of the stem, following fundamental principles of engineering mechanics. Good agreement is found between the field data captured using video-based measurements and the physics-based FE model when a rotational connector element is connected at the base to quantify the 1) relative contribution and moment resistance provided by the root system, 2) displacement at any location along the stalk, and 3) flexural rigidity of the brace-stem system, where the rigidity can be associated with various phenotypes to design plant systems that are more resilient to lateral loading.

Keywords: maize, lodging resistance, digital image correlation, engineering mechanics, finite element model, brace-root system.

Accepted Manuscript
Version of record at: https://doi.org/10.1093/insilicoplants/diac008

Nomenclature

M	$bending\ moment$
E	$Young's\ modulus\ of\ the\ stem$
φ	$curvature$
EI	$flexural\ rigidity\ of\ the\ stem$
I	$moment\ of\ inertia\ of\ the\ stem$
x	$horizontal\ coordinate$
y	$height\ of\ the\ stem$
p	$weight\ of\ head\ spike\ of\ the\ maize\ as\ a\ concentrated\ load$
Q	$wind\ load\ as\ a\ horizontal\ concentrated\ load$
L	$stem\ length$
a	$maximum\ horizontal\ deflection$
x	

1 Introduction

Maize (*Zea mays*) mechanical failure, or lodging, can reduce yield by 3-25% (Carter and Hudelson 1988, Flint-Garcia et al. 2003, Tirado et al. 2020). While many studies recognize the importance and need to understand how plants resist lodging, there are gaps of knowledge on how to efficiently quantify plant failure as a function of plant architecture and plant biomechanics. Further, the majority of work has focused on stalk lodging with limited attention to root lodging or whole plant analyses (Zhang et al. 2012, Chen et al. 2017, Leblicq et al. 2014).

For stalk lodging, studies have revealed an association between biomechanical measures such as stalk breaking strength and stalk flexural stiffness, and the material properties of stalks with stalk lodging-resistance (Robertson et al. 2015). However, previous studies reported large variations in crop stems mechanical parameters such as Young's modulus, tensile strength, bending stress, shear strength, and rigidity modulus (Leblicq et al. 2015, Shah et al. 2017, Karam and Gibson 1994, Alzube et al. 2018, Stubbs et al. 2018, Robertson et al. 2015). This variation can be attributed to the mechanical parameters depending on a wide range of factors such as moisture content, geometry, crop age, genotype, soil type, and nutrition (Leblicq et al. 2015). Hence, understanding mechanical failure of maize plants is not trivial.

In general, the stem contains tissues that have been created from different types of cells; these cells form together to grant the final material of the stems (Shah et al. 2017). X-ray computed tomography (CT) scanning data in conjunction with experimental data was used to generate the geometric analysis of the maize stem (Robertson et al. 2015, Al- Zube et al. 2018), where the cross-section of the maize stem consists of the rind and pith (Figure 1). When the rind has a larger stiffness than the pith, the stem can be modelled as a hollow section (Stubbs et al. 2018).

To measure plant mechanics and link to lodging-resistance, researchers have used various methods to quantify the loading resistance, each relying on a single point application of forces (Robertson et

al. 2015, Sekhon et al. 2020, Reneau et al. 2020, Liu et al. 2012). However, there is a need to evaluate plant mechanics when subjected to dynamic loads, which more accurately reflect the conditions that induce mechanical failure. Further, the stem is often modelled as having a rigid attachment at the base, however stem-borne brace roots at the base of the stalk alter base rigidity (Blizard and Sparks 2018, Hostetler et al., 2021, Reneau et al., 2020).

To understand to what extent the brace roots and root system contribute to lodging resistance in maize, this study deploys a non-contact, vision-based approach to digitally measure the vertical and horizontal displacements of maize stalks with and without brace roots when subjected to simulated wind load to quantify 1) the mechanical properties using fundamental principles of engineering mechanics, and 2) the moment resistance at the base due to the contribution of the brace roots and root system towards providing lodging resistance. Moreover, digital image correlation (DIC) techniques via Imetrum's Dynamic Monitoring Station (DMS) are used to accurately monitor relatively small deformations in a non-contact way to inform structural modelling of the brace roots and root system behavior when subjected to dynamic loads like wind.

2 Materials and Methods

1.1 Field Information

Seeds from CML258 (*Zea mays*; a CIMMYT tropical inbred) were grown in the summer of 2020. CML258 was selected because it is a large and robust inbred line that closely resembles commercial hybrid maize plants, and for the comparison to previous work (Reneau et al. 2020). Seeds were planted on 06/01/2020 in a 60ft by 30ft area containing 60 individual research plots of 18-seeds each at our Newark, DE site (39° 40' N and 75° 45' W). Weather data can be found by selecting the Newark, DE-Ag Farm station on the Delaware Environmental Observing System (http://www.deos.udel.edu). Fields were treated with a pre-emergence (Lexar at 3.5 quart per acre and Simazine at 1.2 quart per acre) and post-emergence (Accent at 0.67 ounces per acre) herbicide. At the time of planting, Ammonium Sulfate (21-0-0 at 90 lbs per acre, fertilizer) and COUNTER 20G

insecticide (at 5.5 lbs per acre) were applied. Approximately 1-month after planting, when plants were at knee high, additional fertilizer was supplied (30% Urea Ammonium Nitrate at 40 gallons per acre). The soil at this location is an Elsinboro silt loam with 3 to 8 percent slopes.

Samples were selected for testing based on their location in the center-most portion of the 60ft by 30ft area. The surrounding plants were cleared to enable placement of the imaging system (DMS). Experimental field testing of the maize inbred CML258 in October 2020 at 124 days after planting was conducted. Four plants with the same genotype were used for the test labelled A, B, C, and D from left to right in the field as shown in Figures 2 and 3. A white PVC board was used as a background to increase the accuracy of the determination of the vertical and horizontal deformation captured by DMS. The wind load was simulated by a whistle fan.

1.2 Simulated wind load

A simulated wind load is generated using a fan located on the ground about three meters (ten feet) away from the side of the plants (Figure 3). The experimental investigation goal was to subject the wind load on the lower part of the maize to capture the corresponding movement of the stalk and brace roots. The average wind height was about one meter (three feet) above the ground. The average temperature was 20.4° C which gives an air density of about 1.2 kg/m^3 (0.075 lb/ft^3) at one atmosphere (1 atm) pressure. The air density at specific height and wind speed can be used to calculate the wind load at that height.

The high fan speed resulted in generating an average velocity between 0 and 24.6 kph (15.3 mph) at a crop height of 0.508 m (20 in) as recorded using a digital anemometer; the ambient wind was included in this reading. According to American Society of Civil Engineers-16 (ASCE7–16), the velocity pressure can be calculated as following equation:

#(1)

where K_z is velocity pressure exposure coefficient, K_{zt} is topographic factor defined, K_d is wind directionality factor, and V is the basic wind speed (section 27.3.2 ASCE 7-16). For this study, K_z is 0.85, assuming the exposure category C, from Table 26.10-1 ASCE 7-16, K_{zt} is 1.0 for homogeneous topography, K_d is 1 (K_d can be ignored for our calculation (Table 26.6-1, ASCE 7-16), K_e is 1 for locations less than 305 m (1,000 ft) in elevation (Section 26.9, ASCE 7-16).

The force that causes the displacement is calculated based on Equation 2:

#(2)

where Q is the force or wind load N or lb, A is the projected area of the object m^2 or ft^2, $P_{pressure}$ is the wind pressure (Equation 1), and C_d is the drag coefficient to account for non-flat surface (1.2 for a long cylinder tube). This force acts normal to the surface and in the direction of the wind (ASCE 7-16). For this study, the wind speed was 24.6 kph (15.3 mph), which translates to a wind pressure of 24.4 N/m^2 (0.51 $lb/ft^{2)}$. A projected area of 0.03 m^2 (0.327 ft^2) was estimated, which produces a wind force equal to 0.89 N (0.2 lb).

Understanding the interaction between wind and maize plants has been a significant challenge, however two models have been proposed: 1) an exponential model where wind speeds are exponentially reduced from the top of the canopy to the base of the plant (e.g. Shaw et al. 1974), or 2) a model in which there is a secondary maximum at the bottom of the canopy that results in monotonic wind profile along with the height of the plant (e.g. Shaw 1976). In maize, wind-induced failure without soil saturation was estimated between 57 and 108 kph (35 and 67 mph) (Wen et al. 2019). Considering this range of wind speeds and an exponential reduction by canopy height, a canopy wind speed of 57-108 kph would expect to drop to 12.3-23 kph (7.6- 14.3 mph) at a measurement height of 0.6m (based on the exponential decay rate estimated from Shaw et al. 1974). The whistle fan is used to generate an initial load to estimate the stem's material properties in the linear, elastic region. This was an adequate amount for the simulated wind load to capture the

brace root influence. We hypothesized that the four plants would behave the same and the wind speed would be equivalent across the four plants, thus, the location of the fan (wind source) has not been changed during the test. However, analysis of the results, as will be discussed in section 4, implies that at farther locations from wind sources with the presence of in-front crops, maize stems would be more susceptible to wind loads. In addition, these in-front maize would change the wind direction that was found to influence the mechanics of the stem, particularly in the context of crosswinds or perpendicular winds.

1.3 Background: Imetrum's Dynamic Monitoring Station (DMS)

DMS is characterized by the versatility of applications such as measuring bridge and rail track deflections with high resolution, real-time high-speed cameras, and Video Gauge™ software. In this study, non-contact structural monitoring of the maize stalk, brace roots and root system was captured using a proprietary system by Imetrum via their DMS with Video Gauge™ software. Digital image correlation (DIC) algorithms were then used to dynamically monitor deflections of maize plants from a simulated wind load in real-time. The DMS functions as a reliable, two-dimensional DIM system (vertical and horizontal measurements) that uses algorithms based on digital image correlation (DIC) and point-to-point tracking to make virtual measurements with accuracies within thousandths of an inch.

The mechanical properties of the samples were first computed based on engineering mechanics using mechanical theories in the linear, elastic region (i.e. small displacements) and deflections measurements captured by the DMS. Then, the deflections are verified by a finite element (FE) model generated using ABAQUS. The deformed shape of the ABAQUS model and displacements along the stem are tracked and compared to the digital image measurements from the field testing as described in more detail in section 4.4.

Virtual displacement gauges were set up within the DMS to measure the vertical and horizontal deflection of the stem, magnitude of this displacement under certain applied lateral load referred to as the flexural rigidity, and structural and material properties of the stem. By combining the non-contact, DIC measurement capabilities from the DMS and engineering mechanics, the modulus of elasticity and the strength resistance of the stem can be estimated by assuming linear behavior for the stem and applying Euler Bernoulli beam theory described in section 2. The horizontal deflection determined by Imetrum's DMS and the mechanical properties (i.e., modulus of elasticity and stiffness) shown in Euler Bernoulli's beam theory provide an estimate of the ultimate load that the stem and root can carry before lodging (i.e. failure). The consequence of removing the brace roots and its influence on uplifting the stalk was calculated using basic geometry (Appendix A).

1.4 Measuring displacement using Imetrum's Dynamic Monitoring Station (DMS)

For this study, two cameras are used to capture 2D deformations—horizontal and vertical displacements when the stalk displaces when subjected to a simulated wind load. Since this study is to quantify the effect of the brace root, the focus of the two tests was approximately on the lower mid-height of the maize. In addition, using a smaller field of view with the DMS enables a higher level of accuracy for point-to-point tracking and digital image correlation. The first round of testing was conducted with intact brace roots for all the samples, and the second round of testing was performed with the brace roots removed from Plant A and C. To capture the displacement, the targets are attached at seven positions on the stem, whilst the brace root carries targets at two positions. The highest target is 0.51 m (20in) above the ground line for Plant A and B, and 0.44 m (17.5 in) for Plant C and D, and all other targets are spaced approximately 0.06 m (2.5 in) apart down. Figure 3 shows the location and designation of the targets where the displacements are recorded along the stem and roots. Each target has a unique designation; the first letter of the designation represents the Plant name, where “A” is Plant A and “C” is Plant C. The second letter “R” denotes the root, and last letter represent “T” for top and “B” for bottom in which the height of the “T” is 0.06 m (2.5 in) where “B” near to the ground. The maximum displacement field data using

DMS focusing on root deformation is shown in Table 2. Two cameras were used for the two tests: Camera 33 and Camera 37, which focused on brace root deformation and stalk deformation, respectively. Figure 3 shows the position of the two cameras, Camera 33 is close to the ground to more focus on the root, while Camera 37 is focused on the stem.

2 Engineering mechanics analysis

Lodging failure mode can be either by: 1) rupture of the root system, 2) anchorage failure via shearing of the soil, whereas shear failure is most likely to govern tall plants, or 3) stalk buckling. Bending and buckling are the common type of failure mechanism for hollow and slender stalks such as maize (Neenan and Spencer 1975; Karam and Gibson 1994). Since the lateral deflection (buckling) is the govern failure mode for the stem, the long stem under loads can be unstable causing the stem to deflect laterally and eventually collapse. Similar to previous studies (Liang and Guo 2008, Brune et al. 2018, Reneau et al. 2020, Stubbs et al. 2020), the flexural behavior of maize has been idealized as a cantilever beam based on Euler-Bernoulli beam theory, assuming small displacement theory.

$$\frac{^{2}(3 \quad y)}{} \left(\frac{}{s(L*(\sqrt{\frac{P}{}}))} \right) \left(\quad \left(y * \sqrt{-} \right) \quad 1 \right) \#(3)$$

where x is the horizontal coordinate (see the x and y directions followed in this study in Figure 1), E is the modulus of elasticity and I is the moment of inertia, P is a vertical load (load of head spike of the maize as a concentrated load), Q is a horizontal concentrated load (simulated wind load shown in Figure 4), L is span length, and (a) is the maximum horizontal deflection due to both loads, y is the height where the deflection is recorded along the stem. Equation 3 can be used to conservatively estimate and understand the mechanical behavior of maize subjected to various loading and provide plant structural design approaches in the case of fixed support. Also, it can lead to understanding a plant's global structural response when subjected to both vertical and horizontal loads. However,

the stem is assumed to not be fully fixed at the base, so rotation at the base exists and needs to be accounted for in the structural response. In fact, some contribution of the deformation due to rotation at the support needs to be accounted for in the theoretical formulation. The additional deflection of a stem experiencing a rotation of θ at the base can be represented as:

#(4)

where x_θ is the deformation due to the rotation at the base, and is the rotation at the base. Therefore, the total deflection at any point along the stem is the sum of the two parts from Equations 3 and 4:

$$\frac{(3 \quad y)}{} \left(\frac{}{(L * (\sqrt{\frac{P}{EI}})} \right) \left(\left(y * \sqrt{\frac{}{}} \right) \quad 1 \right) \qquad \#(5)$$

Equation 5 represents the theoretical formulation using engineering to quantify the moment resistance at the base, which, in turn, can be used to quantify the rotational stiffness of the maize and brace roots when intact and removed. Figure 4 illustrates the resistance moment, M, at the base due to the horizontal and vertical loads, Q and P, respectively.

2.1 Rotational, axial, and flexural stiffness of the stalk in linear elastic region

The stiffness of an elastic member can be designed as the deformation resistance of the member due to external force. It is a material and geometric property (Hibbeler and Kiang 2015). From the displacement measurements in vertical and horizontal direction, both components can be used to

compute the rotational, axial, and flexural stiffness based on the elastic extension and bending moment theories.

Rotational Stiffness: The relative contribution of the root system is captured by the moment resistance provided by the stalk at the base. In addition, the displacement captured by the digital image measurement are used to inform structural modelling and quantify the relative contribution of the root system at the base, which provides moment resistance, M. From the displacements, the rotation, θ, at the base can be computed, which in turn, can be used to approximate the rotational stiffness, K_r, of the root system through the following relationship shown in Equation 6.

$$— \#(6)$$

Axial and flexural stiffness based on elastic extension and bending moment theory: Elastic extension theory can be used to calculate the axial stiffness. In this case, the stalk can be modelled as a single degree of freedom (SDOF) (Figure 5), where the entire stalk is idealized as a cantilever beam with stiffness, K, and constant EI. Data recorded along the longitudinal (vertical) axis of the stem can be used to find the axial stiffness of the stalk. For the Imetrum DMS to accurately track the movement of a point of interest, there must be a contrast between the location of the point of interest and the area around it. These contrasts were created by placing one vinyl adhesive square-shaped bulls-eye target on each point. The difference in the vertical measurement between the target at the brace root when the brace root is intact and then removed (to subtract any uplift) and the height at a target is expressed as the deflection δ(y) shown in Equation 7. Equation 8 can be used to compute the axial stiffness (K_a) along the stem. In Figure 5, y represents the vertical displacement measurement when the brace root is intact, while y' is the vertical reading when the brace root is removed:

$$\delta(y) \quad — \#(7)$$

$$- \quad -- \#(8)$$

where P is the axial load.

From elastic beam theory, the nonsymmetric section in both directions has different moments of inertia, I, in each direction and the flexural rigidity, EI, will increase as the moment of inertia increases. Accordingly, sections with larger flexural rigidity in a certain direction are generally stiffer and can attract larger forces that need to be resisted by the cross-section in that direction. Hence, the bending stiffness is affected more by the loading direction applied to the cross-section. The cross-section of the stem is approximately circular in shape, so the loading direction will not have an effect and the stiffness will be the same under any load direction. In addition, the deflection, δ, depends on the flexural rigidity, EI, and the location of the applied force and its distribution for a given length, L. The flexural stiffness, K, for stalk can be calculated based on the lateral load Q and the length L:

$$- \#(9)$$

3 Verification using finite element modeling

A finite element (FE) model is used to theoretically verify the measured deflections captured from field data. Previous studies (Niklas 1992, Baker 1995, Liang and Guo 2008, Yang et al. 2014, Stubbs et al. 2018) have focused on building mechanical models of the plant using various software programs but agree on limiting the complexity of the components of stems and roots given the difficulty to accurately represent them. In most cases, these components are not modelled explicitly, and approximations about the material properties are made to make the analysis easier and the model less computationally expensive (Liang and Guo 2008).

Suggested parameters for modelling parts of the plant, material properties, boundary conditions, and applied load using ABAQUS (finite element modelling software) are presented where the stem model is assumed to consist of a slender and homogeneous solid beam (Spatz and Speck 2002, Liang and Guo 2008) with a circular cross-section (Liang and Guo 2008). The model height is 0.508 m (20 in) and a circular cross-section radius of 0.025 m (1 in) at the top. Poisson's ratio, υ, is taken as 0.25 for this model (Stubbs et al. 2018). For the simplicity the moment of inertia has been taken to be constant and equal to 0.056 in^4, which is the moment of inertia of the section at the height 0.44 m (17.5 in).

To compute for the self-weight, the mass density is defined to be 127 kg/m^3 (0.005 lb/in^3) (Zhang et al. 2012). For better meshing, the circular cross section of the stem has been partitioned into two concentric circles, which extrude to the entire body of the member. Two concentrated loads, one horizontal and one vertical, were applied to the model. The horizontal loads represent the wind load from the fan and the effect of the deformation due to rotation at the support ($x_\theta=\theta_{base}* y$), where this displacement x_θ converts to a concentrated load applied horizontally at the top. The vertical load is used to simulate the upper part of the stem since the focus is on the bottom 0.44 m (17.5 in) of the stalk and root system. The approximate height of the maize is about 1.57 m (62 in) with an approximate stem diameter of 0.015 m (0.6 in) at the top; however, the focus of this research is on the lower part, where the targets along the stalks were distributed 0.44 m (17.5 in) from the ground. The FE model height was 0.50 m (20 in) and the remaining part of the stalk, approximately 1.06 m (42 in), was converted to a statically equivalent load applied at a reference point at the top of the model using continuum distributing coupling constraints. In other words, the mass from the upper portion was not distributed along the stem but rather idealized as a concentrated load acting on the top pointing in the direction of gravity.

Incompatible mode elements, C3D8I, are used for the model to overcome the issues relating to shear locking. This type of element improves the element's deformation gradient, and is preferred

for members subjected to flexural bending moments. For the boundary condition (BC), two types of BCs are applied on two models: “fixed BC” and “pinned BC”. For the first model, a “fixed BC” is applied to a reference point at the center of the cross-section with a continuum distributing coupling. For the second model, the “fixed BC” is removed, then a basic connector element is applied to the reference point using a wire feature connecting to the ground to simulate a pinned support where rotation is not restrained. The available components for the relative motion for the connection section are the rotations in 3-directions using “Join” for the translational type and “Rotation"” for the rotational type.

4 Results

4.1 Plant phenotypic analysis

Previous research has shown that plants can produce a different result for the loading resistance strength whether considering a single stalk or population (Liu et al. 2012); as such, lodging resistance can be represented more accurately by the population lodging resistance strength and not the single stalk lodging resistance strength. Therefore, four consecutive plants are selected for analysis Plant A, B, C, and D (Figures 2 and 3). These plants had similar phenotypes, with identical number of brace root whorls in the soil and stem diameters, similar brace root number, brace root diameter and brace root length (Table 1).

4.2 Wind displacement of stalks over time with brace roots intact

CML258 plants were subjected to a simulated wind load and stalk displacements were measured at various points along the stem. Figure 6 shows the displacement time history of the stem behavior from the DMS test when the brace roots are intact (Table 2, Test 1) for all samples subjected to maximum wind speeds up to 24.6 kph (15.3 mph). The total time for the test is 28s, where the

horizontal displacement was captured by the DMS for Plant A, B, C, and D at a height of 0.44 m (17.5 in) with a data sampling rate of 50Hz.

Since no action was taken to reduce the swirl from the fan, there was turbulence introduced. The turbulence was exacerbated by the presence of the first windward plant. The frequency patterns of the four plants were out-of-phase and in-phase in the positions. From Figure 6, it is shown that the deformation pattern of the two plants closest to the wind source (Plants A and B) were out-of-phase with Plants C and D, which do not reach their peaks at the same time. The two plants farther from the source (Plants C and D) deform opposite from the source of wind, where positive values in the dataset represent the deformation that opposes the wind source. This is an indication that the dominant deformation pattern for the two plants closest to the wind source and other plants (Plants C and D) are out-of-phase during this loading sequence. The two plants closest to the source (Plants A and B) experience smaller deformations than the two plants that are farther from the source (Plants C and D). These results highlight the complex and multi-directional force profiles the plant encounters even from a simple wind point source.

From the DMS data, and using Equation 5 for combination vertical and horizontal load, the calculated flexural rigidity, EI, of the four plant stems when the brace root is intact using the DMS is shown in Table 2. Including the vertical load and the rotation at the base will maximize the base moment, especially when the brace roots are removed since the horizontal deflection is greater (as it was described in section 2) which makes the moment arm for the vertical load larger.

4.3 Wind displacement of stalks over time with brace roots removed

Unsurprisingly, the horizontal displacement of the stem with the brace root removed is greater than with brace roots intact; Figure 7 shows the large displacement amplitude when brace roots are excised for Plant C, which can affect the stiffness of the stalk in the linear elastic region. From Table 2, Plant A experienced larger deformation than Plant C when the brace roots were removed, and

that was likely because of the brace root geometry for both Plants A and C. The brace roots for A were larger and thicker so when they were removed, it made a larger difference in terms of the stability of the stalk. Recall that when brace roots were intact, Plants A and B exhibited less deflection than Plants C and D; thus, these differences were unlikely to be due to the wind itself.

Using the DMS data to calculate the rotational stiffness, it was found that the stem of Plant A has 97% less rotational stiffness after brace root removal. For Plant C, the rotational stiffness is 82% less without the brace roots than with the brace root. The data show that brace roots are important to increase rotational stiffness and limit stalk deflection. Since the wind speed is the same for both tests (with brace root and without), it can be assumed that P, axial, load, is the same in both cases. By adding the vertical displacement that is recorded using the DMS, L_o is increased by 0.05 m (2.06 in) when the brace root is removed for Plant A, and 2.02 for Plant C. The axial stiffness for the stalk is 10.7% less when the brace roots are removed. The stem of Plant A has 85% less flexural stiffness without the brace roots than with them. For Plant C, the stem is 42% less stiff without the brace roots than with the brace root.

Removing the brace roots has no effect on the properties of the stalk; hence any differences in the data are related to a change in the stability presented by the presence of the brace root (Reneau et al. 2020). The uplift is about 10 times higher than the uplift when the brace root is intact. For Plant A, the target moves from the ground by $1.2*10^{-3}$ m (0.05 in) at target A1 after being subjected to wind load about 24.6 kph (15.3 mph) for 90 sec when the brace roots are removed, noting the soil was not saturated. For Plant C, the target moves from the ground by $6*10^{-4}$ m (0.027 in) at target C2 after being subjected to wind load of about 24.1 kph (15 mph) for 8 sec. From this result, it can be concluded that the brace roots limit both horizontal and vertical displacement of the stalk (Table 2). The results presented in table 2 and explained in section 2) show that the role of the brace root to the rigid base (i.e. stalk anchorage), which provides lateral resistance and limit stalk deflection.

4.4 Deformation finite element (FE) modelling result

The model describes the behavior of the crop stem when it is subjected to horizontal and vertical load. Figure 8 shows a mechanical model of the stem subjected to a concentrated load in the x-direction and vertical load at height 0.50 m (20 in). This deformed shape and horizontal displacement correspond to a test with brace root intact for Plant A. Table 3 shows the comparison between the DMS data and the ABAQUS finite element (FE) model. The FE model with the modulus of elasticity calculated based on including both vertical and horizontal load (Equation 5) produced lateral displacements within 90.3% agreement of the video-based displacement measurements obtained by the DMS. In addition, the ABAQUS analysis included the effect of deflection and rotation which were already captured by DMS. The displacement along the stem of Plant A from the finite element model is compared to the experiment data, DMS, and theoretical equations, shown in Table 4 and Figure 9. Modelling the interaction between the stalk and soil as rigid, however, provides a stiffer model than the actual behavior of the plant. Moment resistance occurs at the base but is not totally rigid given the non-rigid soil and root properties; thus, the plant is not rigidly connected to the ground as a conventional “fixed” or “rigid” support would imply. Good agreement is found between the model and field data captured by the DMS when the model includes a connector element to simulate a pinned support at the base.

Equation 3 provides a stiffer response than results from the DMS because of the assumed “fixed” boundary condition in Equation 3. In addition, using Equation 5 gives a result closer to the results obtained from the ABAQUS model when the boundary conditions at the base are not “fixed” or “rigid” (Figure 9). Therefore, it follows that the rotation at the base cannot be ignored nor assumed to be fully “fixed” or “rigid.” Hence, Equation 5 shows a theoretical formulation of the mechanical behavior of maize based on engineering mechanics when the stem is subjected to both vertical and horizontal loads.

In summary, the results show the presence of the two plants farther from the source (Plants C and D) can cause a negative pressure acting on plants closer to the wind source; this finally results in the out-of-phase movement for all plants. The application of the DMS in this study helped to monitor the deformation of the stem using a non-contact, vision-based approach. Video post-processing of the dynamic response enables closer observation of the deformations and suggests how the effects of turbulence may appear; future studies to repeat these tests within a wind tunnel to generate realistic wind load effects are recommended. The effect of the wind speed also differed between the plants given the differences of the brace roots systems and interaction between the brace roots and the soil. A significant relationship was observed between the deformation and the brace roots system—small displacements were captured when brace roots were attached to the stem, while displacements were larger when brace roots were removed. Thus, irrespective of brace root geometry such as the number of whorls, number of roots per whorl, thickness, and length, removing the brace roots increased the axial and lateral deformation of the stalk to a similar extent. The rotational, axial, and flexural stiffness were associated for the most part with the brace roots system. Subjecting the maize to wind load for a duration of time can cause uplift, which may result in a weak intersection between the roots and the soil and consequently have an additional effect on lodging. Instead of assuming a rigid attachment at the base, it was suggested for the end support to be pinned in a form of a connector element (spring) in ABAQUS to mimic the rotational stiffness provided by the brace root and root system. Information gained from field testing using video-based measurements provides insight as to how to characterize the mechanical behavior of maize and its brace root system (above and below ground) using engineering mechanics.

5 Conclusions and future research

The root and stem displacement of maize were observed and recorded using DMS. The maize plants were subjected to simulated wind load in the field to evaluate the contribution of the brace root on securing the maize's stem at the base using a linear analysis. Euler-Bernoulli's beam theory was applied to calculate the flexural rigidity, EI, of the stem by assuming small displacements. The simulated wind load was idealized as a statically equivalent load on the stem to apply engineering mechanics to analyze the system. On the basis of the presented experimental research, the following conclusions can be made:

- The investigation shows the impact of plant-induced turbulence on deflection. These results highlight the complex and multi-directional force profiles the plant encounters even from a simple point-source of wind.
- Displacements that were captured when brace roots were removed were larger than when the brace roots were intact for the stem for both Plants A and C.
- Quantifying the effect of the brace roots was achieved where this study confirms that the brace roots contribute to the moment resistance at the base (i.e. stalk anchorage), which provides lateral resistance and limits stalk deflection.
- Removing the brace root in the base of the stalk decreased the rotational, axial, and flexural stiffness for the stalk. However, removing the brace root can increase the uplift of the stalk from the ground up to ten times compared to the uplift for stalk with the brace root intact.
- For accurate FE modelling, the base is not completely "fixed" or "rigid," which implies no rotation at the base. Rather, rotational restraint at the base is provided in part by the stalk's flexural stiffness in conjunction with the brace root and root system, and modelled with a pinned support. This adjusted boundary conditions at the base produced lateral displacements within 9.7% error when compared to non-contact, video-based displacement measurements obtained by the DMS with displacements on the order of ~0.001 inch.

- This approach can be used to understand the flexural rigidity of the brace-stem system, where the rigidity can be associated with various phenotypes to design plant systems that are more resilient to lateral loading.

Future testing can be conducted to estimate shear strains to determine shear modulus and shear stresses using DMS. Shear stress is the result of a force that tends to cause deformation of the maize stem by slippage along a plane parallel to the stem's cross-section. In addition, more field data could be collected to explain variable wind speeds and observe the movement of the plants with the simulated wind at various positions to look at both in-plane and out-of-plane deformations. More simulations can be conducted with the ABAQUS model to analyze other architectures and genotypes. The FE model serves as a baseline model that can be used for parametric analyses to conduct with more confidence and provides a more comprehensive parametric study. Such a model (i.e, maize model) can be used to predict how to save the crops from destruction and explore several failure modes within a common model.

ACKNOWLEDGMENTS

The authors would like to express gratitude to Jonathan Reneau for assistance in the field and Sydney Ross for editing the manuscript prior to final submission. Also, the authors would like to express gratitude to Dr. Ashley Hostetler for reviewing the manuscript. We thank Lindsay Erndwein of Illustrations by LindZeaMays for illustrating Figure 5 of this article. Research funding was provided by the University of Delaware Research Foundation (UDRF) Strategic Initiative Grant to Erin E. Sparks and Monique H. Head to support this multidisciplinary research effort.

References

Ambrose, J., & Vergun, D. (1997). Simplified building design for wind and earthquake forces (Vol. 29). John Wiley & Sons.

Al-Zube, L., Sun, W., Robertson, D., & Cook, D. (2018). The elastic modulus for maize stems. Plant Methods, 14(1), 11.

ABAQUS CAE. N/A: ABAQUS Inc., 2019.

Ashby, M. F., Shercliff, H., & Cebon, D. (2018). Materials: engineering, science, processing and design. Butterworth-Heinemann.

American Society of Civil Engineers. (2017, June). Minimum design loads and associated criteria for buildings and other structures. American Society of Civil Engineers.

Bauer, F., 1964. Some indirect methods of determining the standing ability of wheat. Z. Acker Pflanzenbau. 119, 70–80

Briggs, K.G., 1990. Studies of recovery from artificially induced lodging in several six-row barley cultivars. Can. J. Plant Sci. 70, 173–181.

Blizard, S., & Sparks, E. E. (2018). Maize nodal roots. Annual Plant Reviews online, 281-304.

Baker, C. J. (1995). The development of a theoretical model for the windthrow of Plants. Journal of Theoretical Biology, 175(3), 355-372.

Brune, P. F., Baumgarten, A., McKay, S. J., Technow, F., & Podhiny, J. J. (2018). A biomechanical model for maize root lodging. Plant and soil, 422(1), 397-408.

Boresi, A. P., Schmidt, R. J., & Sidebottom, O. M. (2003). Advanced mechanics of materials (Vol. 6). New York: Wiley.

Crook, M.J., Ennos, A.R., 1994. Stem and root characteristics

Coulbourne, W. L., & Stafford, T. E. (2020, April). Wind Loads: Guide to the Wind Load Provisions of ASCE 7-16. American Society of Civil Engineers.

Carter, P. R., & Hudelson, K. D. (1988). Influence of simulated wind lodging on corn growth and grain yield, Journal of Production Agriculture, 1, 295–299. https://doi.org/10.2134/jpa19 88.0295

Dupuy, L. X., Fourcaud, T., Lac, P., & Stokes, A. (2007). A generic 3D finite element model of tree anchorage integrating soil mechanics and real root system architecture. American Journal of Botany, 94(9), 1506-1514.

Flint-Garcia, S. A., Jampatong, C., Darrah, L. L., & McMullen, M. D. (2003). Quantitative trait locus analysis of stalk strength in four maize populations. Crop Science, 43, 13–22. https://doi.org/10.2135/ crops ci2003.0013

Hunter, J. W., & Dalbey, N. E. (1937). A histological study of stalk-breaking in maize. American Journal of Botany, 492-494.

Hibbeler, R. C., & Kiang, T. (2015). Structural analysis. Upper Saddle River: Pearson Prentice Hall.

Harrington, J.B., Waywell, C.G., 1950. Testing resistance to shattering and lodging in cereals. Sci. Agric. 30, 51–60.

Hostetler, Ashley N., Erndwein, Lindsay, Reneau, Jonathan W., Cantera, William, Stager, Adam Tanner, Herbert G., Cook, Douglas, & Sparks, Erin E. (2021). Brace root phenotypes predict root lodging susceptibility and the contribution to anchorage in maize.

Imetrum. https//www.imetrum.com

Karam, G. N., & Gibson, L. J. (1994). Biomimicking of animal quills and plant stems: natural cylindrical shells with foam cores. Materials Science and Engineering: C, 2(1-2), 113-132.

Kelbert, A. J., Spaner, D., Briggs, K. G., & King, J. R. (2004). Screening for lodging resistance in spring wheat breeding programmes. Plant Breeding, 123(4), 349-354.

Liang, L., & Guo, Y. (2008, October). Finite Element Analysis of Single Wheat Mechanical Response to Wind and Rain Loads. In International Conference on Computer and Computing Technologies in Agriculture (pp. 841-846). Springer, Boston, MA.

Leblicq, T., Vanmaercke, S., Ramon, H., & Saeys, W. (2015). Mechanical analysis of the bending behaviour of Plant stems. Biosystems Engineering, 129, 87-99.

Liu, S., Song, F., Liu, F., Zhu, X., & Xu, H. (2012). Effect of Planting density on root lodging resistance and its relationship to nodal root growth characteristics in maize (Zea mays L.). Journal of Agricultural Science, 4(12), 182. https://doi.org/10.5539/jas.v4n12 p182

Murphy, H.C., Petr, F., Frey, K.J., 1958. Lodging resistance studies in oats. Agric. J. 50, 609–611

Niklas KJ (1992) Plant biomechanics: An engineering approach to plant form and function. University of Chicago press, Chicago

Neenan, M., & Spencer-Smith, J. L. (1975). An analysis of the problem of lodging with particular reference to wheat and barley. The Journal of agricultural science, 85(3), 495-507.

Navabi, A., Iqbal, M., Strenzke, K., Spaner, D., 2006. The relationship between lodging and plant height in a diverse wheat population. Can. J. Plant Sci. 86, 723–726.

Rajkumara, S. (2008). Lodging in cereals-a review. AGRICULTURAL REVIEWS-AGRICULTURAL RESEARCH COMMUNICATIONS CENTRE INDIA, 29(1), 55.

Robertson, D. J., Julias, M., Gardunia, B. W., Barten, T., & Cook, D. D. (2015). Corn stalk lodging: a forensic engineering approach provides insights into failure patterns and mechanisms. Crop Science, 55(6), 2833-2841.

Reneau, J. W., Khangura, R. S., Stager, A., Erndwein, L., Weldekidan, T., Cook, D. D., ... & Sparks, E. E. (2020). Maize brace roots provide stalk anchorage. Plant direct, 4(11), e00284.

Shah, D. U., Reynolds, T. P., & Ramage, M. H. (2017). The strength of Plants: theory and experimental methods to measure the mechanical properties of stems. Journal of experimental botany, 68(16), 4497-4516.

Stubbs, C. J., Baban, N. S., Robertson, D. J., Alzube, L., & Cook, D. D. (2018). Bending stress in Plant stems: models and assumptions. In Plant Biomechanics (pp. 49-77). Springer, Cham.

Stubbs, C. J., Oduntan, Y. A., Keep, T. R., Noble, S. D., & Robertson, D. J. (2020). The effect of plant weight on estimations of stalk lodging resistance. Plant methods, 16(1), 1-18.

Sterling, M., Baker, C. J., Berry, P. M., & Wade, A. (2003). An experimental investigation of the lodging of wheat. Agricultural and Forest Meteorology, 119(3-4), 149-165.

Simiu, E., Letchford, C., Isyumov, N., Chowdhury, A. G., & Yeo, D. (2013). Assessment of ASCE 7-10 standard methods for determining wind loads. Journal of Structural Engineering, 139(11), 2044-2047.

Shaw, R. H., Den Hartog, G., King, K. M., & Thurtell, G. W. (1974). Measurements of mean wind flow and three-dimensional turbulence intensity within a mature corn canopy. Agricultural Meteorology, 13(3), 419-425.

Shaw, R. H. (1977). Secondary Wind Speed Maxima Inside Plant Canopies. Journal of Applied Meteorology (1962-1982), 16(5), 514–521. http://www.jstor.org/stable/26178087

Sharma, S., & Carena, M. J. (2016). 'BRACE: A method for high throughput maize phenotyping of root traits for short-season drought tolerance. Crop Science, 56(6), 2996–3004. https://doi.org/10.2135/cropsci2016.02.0116

Shi, J., Drummond, B. J., Habben, J. E., Brugire, N., Weers, B. P., Hakimi, S. M., Lafitte, H. R., Schussler, J. R., Mo, H., Beatty, M., & Zastrow-Hayes, G. (2019). Ectopic expression of ARGOS8 reveals a role for ethylene in root-lodging resistance in maize. The Plant Journal, 97(2), 378–390.

Spatz, H. C., & Speck, O. (2002). Oscillation frequencies of tapered plant stems. American Journal of Botany, 89(1), 1-11.

Tams, A. R., Mooney, S. J., & Berry, P. M. (2004). The effect of lodging in cereals on morphological properties of the root-soil complex. Proceedings of the SuperSoil.

Tirado, S. B., Hirsch, C. N., & Springer, N. M. (2020). Utilizing temporal measurements from UAVs to assess root lodging in maize and its impact on productivity. biorXiv. https://doi.org/10.1101/2020.05.21.108746

Wang, Y., Li, Z.H., 1997. Study on culm quality in wheat cultivar. Triticeae Crop. 17, 28–31 (in Chinese).

Wen, W., Gu, S., Xiao, B., Wang, C., Wang, J., Ma, L., ... & Guo, X. (2019). In situ evaluation of stalk lodging resistance for different maize (Zea mays L.) cultivars using a mobile wind machine. Plant methods, 15(1), 1-16.

Yang, M., Défossez, P., Danjon, F., & Fourcaud, T. (2014). Tree stability under wind: simulating uprooting with root breakage using a finite element method. Annals of botany, 114(4), 695-709.

Xu, Q., Yuan, Z., & Sun, C. (2014, May). Finite element analysis model of wheat lodging resistance. In The 26th Chinese Control and Decision Conference (2014 CCDC) (pp. 3895- 3899). IEEE.

Zhang, Y., Ghaly, A. E., & Li, B. (2012). Physical properties of corn residues. American Journal of Biochemistry and Biotechnology, 8(2), 44-53.

Figure 1 Rind and pith of the maize stem

Figure 2 Four maize plants of the CML258 inbred genotype and brace roots intact were subjected to simulated wind load (a) sketch showing the location and designation of nodes and brace root nodes (b) digital image from the DMS with blue arrows where the displace

Figure 3 Experimental setup and the position of the two cameras 33 (bottom) and 37 (top) for the DMS

Figure 4 Cantilever beam subjected to horizontal and axial load

Figure 5 Single degree of freedom (SDOF) model system

Figure 6 Displacement time history for stem deformation when brace roots are intact (height 0.44 m (17.5 in))

Figure 7 Effect of brace roots system on maize, Plant C, height 0.44m (17.5in)

Figure 8 Mechanical model of the stem subjected to a concentrated load in the x-direction at a height of 0.50 m (20 in) and the connector element to simulate a pinned support at the base

Figure 9 Horizontal displacement vs. stem height data comparison for Plant A

Table 1 Phenotypic data for Plants A, B, C, and D

Sample Designation	number of soil brace root whorls-count	brace roots per whorl-count (Average)	diameter for brace roots-m.10^{-3} (in) (Average)	length of brace roots-m (in) (Average)	stem diameter- m (in)
Plant A	2	22	7.1 (0.28)	0.073 (2.90)	0.025 (1)
Plant B	2	26	6.6 (0.26)	0.056 (2.20)	0.025 (1)
Plant C	2	20	5.3 (0.21)	0.055 (2.18)	0.025 (1)
Plant D	2	20	5.8 (0.23)	0.064 (2.55)	0.025 (1)

Accepted Manuscript
Version of record at: https://doi.org/10.1093/insilicoplants/diac008

Table 2 Experimental test details, the effect of the brace root on horizontal displacements (stem maximum horizontal displacement (x) at height 0.44m (17.5 in) and roots maximum horizontal displacement (x_{roots})), test result using DMS (flexural rigidity, EI, Eq. 3)), rotational stiffness (K_r), axial stiffness (K_a), flexural stiffness (K), and vertical (uplift) displacements)

Test No.	Sample Designation	Brace Roots System	x, m (in)	§§ x_{roots}, $m.10^{-4}$ (in)	⍰ EI, $N.m^2$ ($lb.in^2$)	K_r, N.m/° (lb.in/°)	K_a, N/m (lb/in)	K, N/m (lb/in)	uplift, $m.10^{-4}$ (in)
Test 1	Plant A	intact	0.034 (1.34)	0.50 (0.002)	1.05 (366)	10.2 (90)	50962 (291)	25.0 (0.143)	1.00 (0.0040)
	Plant B		0.037 (1.47)	⍰⍰ ---	0.95 (332)	⍰⍰ ---	53238 (304)	22.7 (0.130)	⍰⍰ ---
	Plant C		0.130 (5.07)	2.00 (0.009)	0.28 (98)	2.30 (20)	13135 (75)	7.80 (0.045)	0.60 (0.0024)
	Plant D		0.160 (6.18)	1.47 (0.006)	0.24 (82)	3.20 (28)	13484 (77)	5.60 (0.032)	9.50 (0.0390)
§Test 2	Plant A	removed	0.250 (9.83)	10.0 (0.071)	---	0.31 (2.8)	45533 (296)	3.50 (0.020)	12.0 (0.0500)
	Plant C		0.220 (8.93)	13.0 (0.053)	---	0.42 (3.7)	11734 (67)	4.55 (0.026)	6.80 (0.0270)

§The brace roots for Plants B and D did not remove for test 2, for this reason, they are not included in the table.

§§For brace root horizontal x-displacement, the measurements were at target ART for Plant A and CRT for Plant C (Fig. 4)

⍰ Flexural rigidity is calculated based on the first test when the brace roots are intact.

⍰⍰ Data was not captured due to unanticipated limitations in the field of view or human error.

Table 3 Comparison between the DMS data and the ABAQUS model with varying support conditions

Plant name	Displacements at stem height, y = 0.44 m (17.5 in)		
	ABAQUS FEM-Pinned	DMS	ABAQUS FEM-Fixed
	m (in)		
Plant A	0.037 (1.47)	0.034 (1.34)	0.033 (1.30)
Plant B	0.040 (1.58)	0.037 (1.47)	0.034 (1.34)
Plant C	0.127 (5.01)	0.129 (5.07)	0.077 (3.05)
Plant D	0.151 (5.97)	0.157 (6.18)	0.922 (3.63)

Accepted Manuscript
Version of record at: https://doi.org/10.1093/insilicoplants/diac008

Table 4 Comparison of the experimental and FE data along the stem for Plant A

Target designation	Stem height (y)	ABAQUS FEM-Pinned	DMS	ABAQUS FEM- Fixed	Theoretical Equation (Equation 3)	Theoretical Equation (Equation 5)
	m (in)					
ART	0.06 (2.50)	0.001 (0.05)	$5.0*10^{-5}$ (0.002)	$7.6*10^{-4}$ (0.03)	$7.5*10^{-4}$ (0.03)	$1.25*10^{-3}$ (0.05)
A1	0.13 (5.00)	0.004 (0.17)	§$1.14*10^{-13}$	$2.7*10^{-3}$ (0.11)	0.003 (0.12)	$4.0*10^{-3}$ (0.16)
A2	0.19 (7.50)	0.008 (0.34)	$8.7*10^{-3}$ (0.35)	0.006 (0.26)	0.006 (0.27)	$8.0*10^{-3}$ (0.32)
A3	0.25 (10.0)	0.014 (0.56)	0.014 (0.59)	0.011 (0.46)	0.011 (0.46)	0.013 (0.53)
A4	0.31 (12.5)	0.020 (0.82)	0.020 (0.80)	0.017 (0.70)	0.017 (0.69)	0.019 (0.78)
A5	0.37 (15.0)	0.028 (1.13)	0.026 (1.06)	0.025 (0.99)	0.023 (0.94)	0.026 (1.05)
§§A6	0.44 (17.5)	0.037 (1.47)	0.033 (1.34)	0.033 (1.30)	0.030 (1.22)	0.033 (1.34)

Figure 1

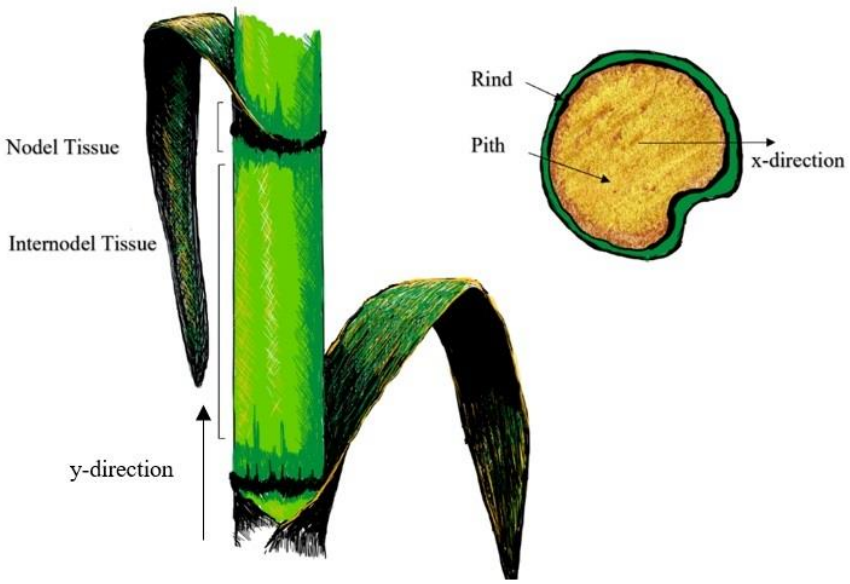

Accepted Manuscript
Version of record at: https://doi.org/10.1093/insilicoplants/diac008

Figure 2

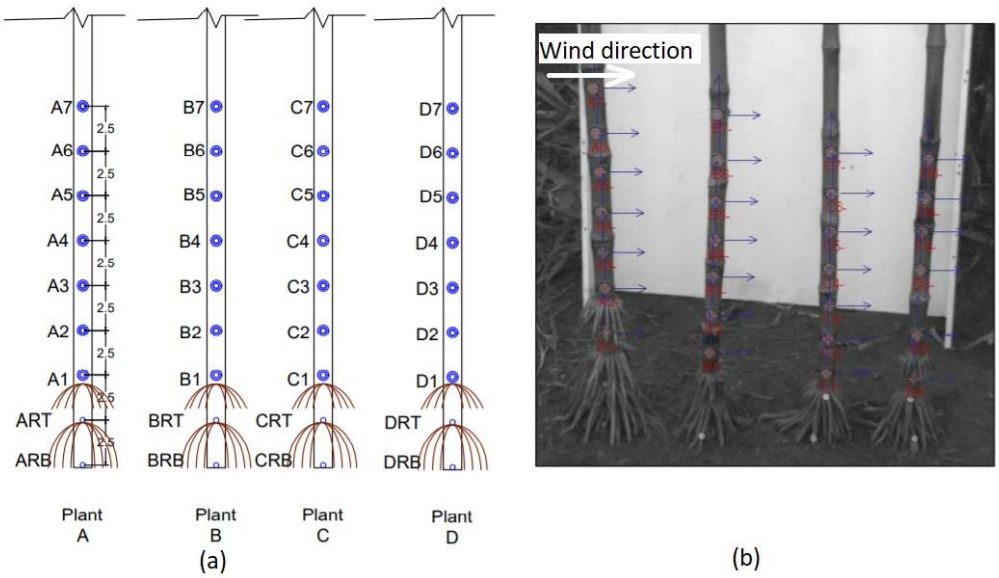

Figure 3

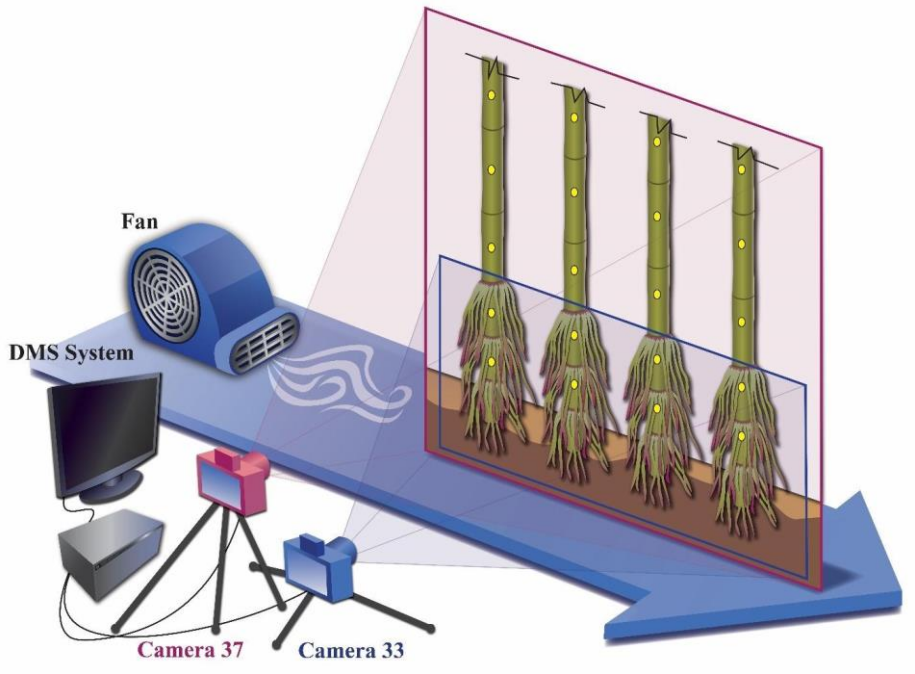

Accepted Manuscript
Version of record at: https://doi.org/10.1093/insilicoplants/diac008

Figure 4

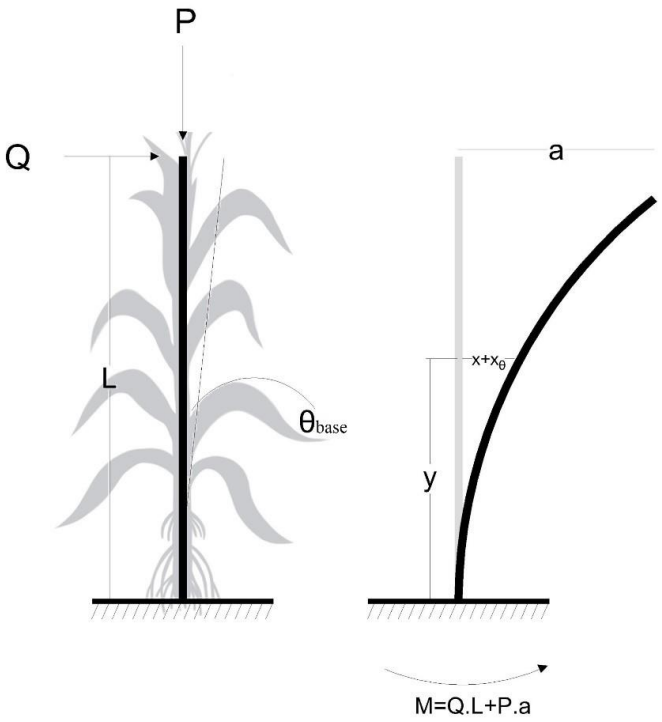

Accepted Manuscript
Version of record at: https://doi.org/10.1093/insilicoplants/diac008

Figure 5

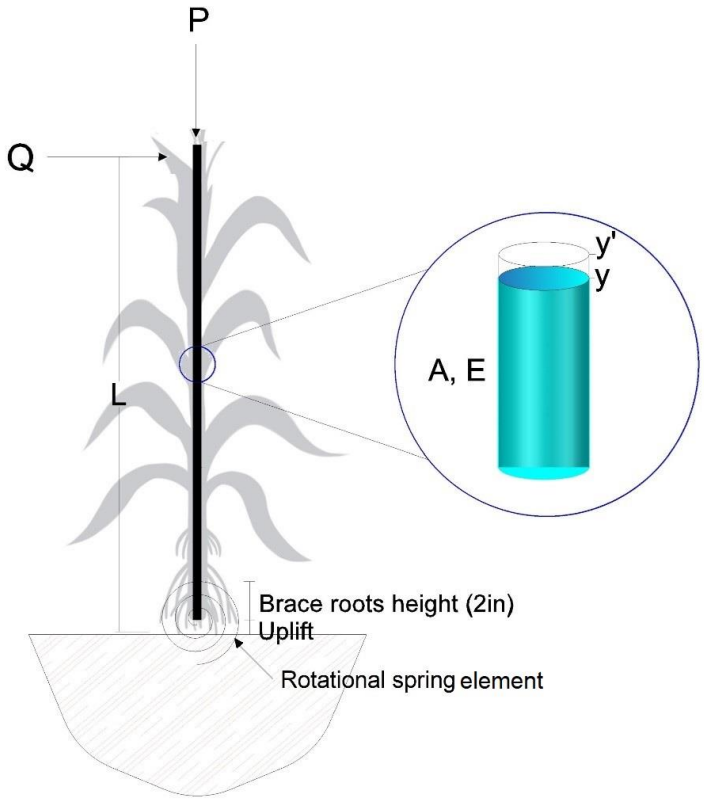

Accepted Manuscript
Version of record at: https://doi.org/10.1093/insilicoplants/diac008

Figure 6

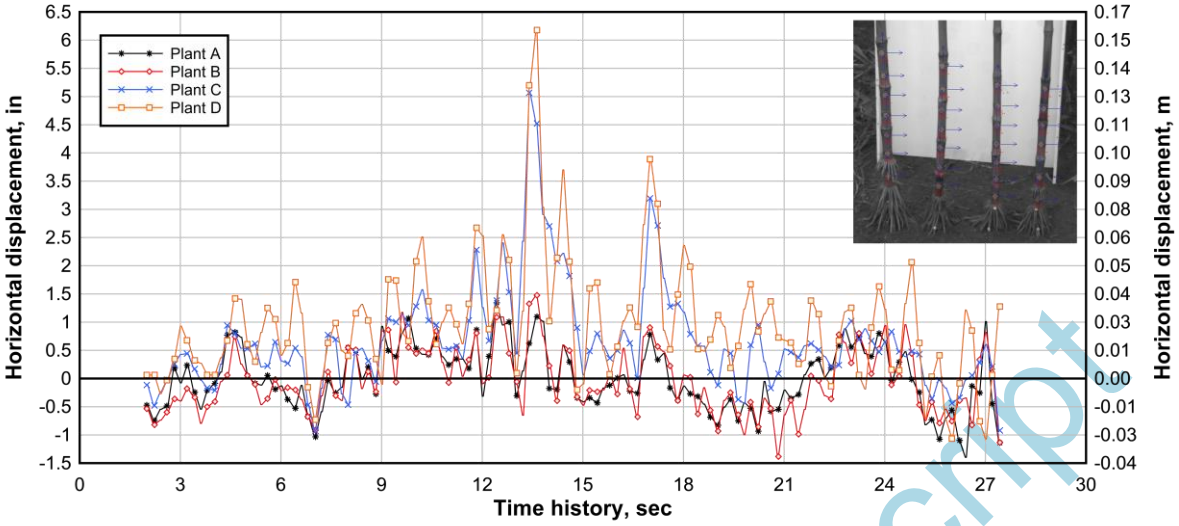

Figure 7

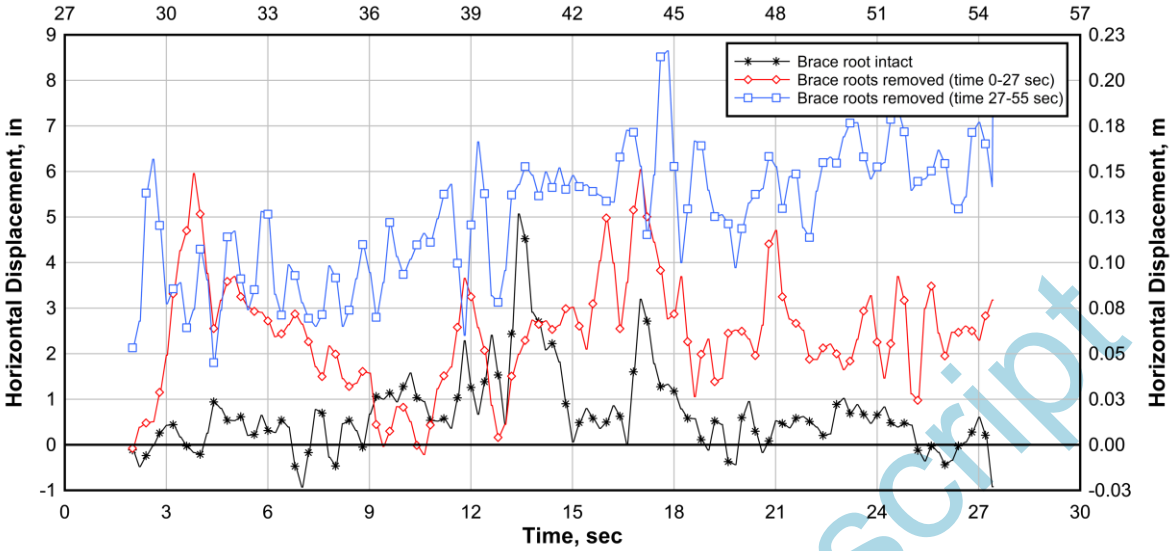

Accepted Manuscript
Version of record at: https://doi.org/10.1093/insilicoplants/diac008

Figure 8

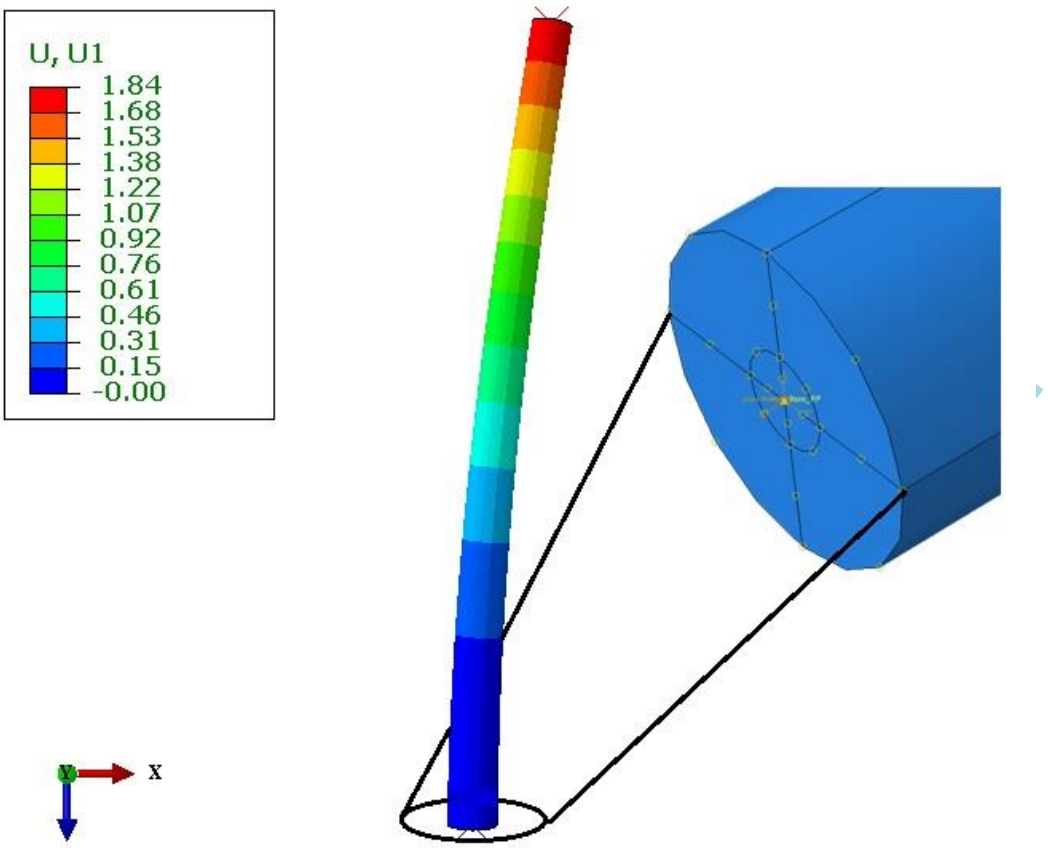

Accepted Manuscript
Version of record at: https://doi.org/10.1093/insilicoplants/diac008

Figure 9